

## Article

# Metabolic Changes in Maternal and Cord Blood in One Case of Pregnancy-Associated Breast Cancer Seen by Fluorescence Lifetime Imaging Microscopy

Li Zhou <sup>1,2</sup>, Yawei Kong <sup>1</sup>, Junxin Wu <sup>1</sup>, Xingzhi Li <sup>3</sup>, Yiyan Fei <sup>1</sup> , Jiong Ma <sup>1,4,5</sup> , Yulan Wang <sup>6,\*</sup> and Lan Mi <sup>1,4,\*</sup> 

- <sup>1</sup> Shanghai Engineering Research Center of Ultra-Precision Optical Manufacturing, Key Laboratory of Micro and Nano Photonic Structures (Ministry of Education), Department of Optical Science and Engineering, School of Information Science and Technology, Fudan University, 220 Handan Road, Shanghai 200433, China; zhou116@fudan.edu.cn (L.Z.); 18110720005@fudan.edu.cn (Y.K.); 18210720098@fudan.edu.cn (J.W.); fyy@fudan.edu.cn (Y.F.); jiongma@fudan.edu.cn (J.M.)
- <sup>2</sup> Department of Biochemistry and Molecular Biology, School of Life Sciences, Fudan University, 220 Handan Road, Shanghai 200433, China
- <sup>3</sup> School of Materials Science and Engineering, Hubei University of Automotive Technology, 167 Checheng West Road, Shiyan 442002, China; 20010037@huat.edu.cn
- <sup>4</sup> Institute of Biomedical Engineering and Technology, Academy for Engineer and Technology, Fudan University, 220 Handan Road, Shanghai 200433, China
- <sup>5</sup> Shanghai Engineering Research Center of Industrial Microorganisms, The Multiscale Research Institute of Complex Systems (MRICS), School of Life Sciences, Fudan University, 220 Handan Road, Shanghai 200433, China
- <sup>6</sup> Department of Gynecology and Obstetrics, The Central Hospital of Wuhan, Tongji Medical College, Huazhong University of Science and Technology, 26 Shengli Str., Wuhan 430014, China
- \* Correspondence: wangyulan@zxhospital.com (Y.W.); lanmi@fudan.edu.cn (L.M.)



**Citation:** Zhou, L.; Kong, Y.; Wu, J.; Li, X.; Fei, Y.; Ma, J.; Wang, Y.; Mi, L. Metabolic Changes in Maternal and Cord Blood in One Case of Pregnancy-Associated Breast Cancer Seen by Fluorescence Lifetime Imaging Microscopy. *Diagnostics* **2021**, *11*, 1494. <https://doi.org/10.3390/diagnostics11081494>

Academic Editor: Antonio Maccio

Received: 17 June 2021

Accepted: 16 August 2021

Published: 19 August 2021

**Publisher's Note:** MDPI stays neutral with regard to jurisdictional claims in published maps and institutional affiliations.



**Copyright:** © 2021 by the authors. Licensee MDPI, Basel, Switzerland. This article is an open access article distributed under the terms and conditions of the Creative Commons Attribution (CC BY) license (<https://creativecommons.org/licenses/by/4.0/>).

**Abstract:** Pregnancy-associated breast cancer (PABC) is a rare disease, which is frequently diagnosed at an advanced stage due to limitations in current diagnostic methods. In this study, fluorescence lifetime imaging microscopy (FLIM) was used to study the metabolic changes by measuring maternal blood and umbilical cord blood via the autofluorescence of coenzymes, reduced nicotinamide adenine dinucleotide (phosphate) (NAD(P)H), and flavin adenine dinucleotide (FAD). The NAD(P)H data showed that a PABC case had significant differences compared with normal cases, which may indicate increased glycolysis. The FAD data showed that both maternal and cord blood of PABC had shorter mean lifetimes and higher bound-FAD ratios. The significant differences suggested that FLIM testing of blood samples may be a potential method to assist in PABC non-radiative screening.

**Keywords:** pregnancy-associated breast cancer; blood; fluorescence lifetime imaging microscopy; NAD(P)H; FAD

## 1. Introduction

According to the updated global cancer statistics 2020, breast cancer is one of the most frequent malignancies and the leading cause of cancer death in females worldwide [1]. The clinical situation can be more complex with pregnancy-associated breast cancer (PABC), which is defined as breast cancer diagnosed during pregnancy or within the first 12 months postpartum. The overall incidence of PABC is low—about 6.5 cases per 100,000 births [2]. PABC is one of the most serious threats to pregnant women; however, the extremely low probability may lead to negligence in self-detection and clinical examination. Moreover, normal physiological changes in the breast, such as engorgement and tenderness, frequently happen during pregnancy, which increases the difficulty of diagnosis of PABC by physical imaging. Ultrasound and mammography are recommended to evaluate a breast mass. Even though ultrasound has a sensitivity close to 100%, it brings a high negative prediction

rate [3]. Mammography is used for further detection and characterization, but research has shown that it is less sensitive, detecting 86.7% of cases of PABC, and it poses a radiation risk to fetus and pregnant patient [4]. In another cohort study, women below 40 years old who underwent PABC had more aggressive subtypes, such as triple-negative breast cancer up to 5 years after parturition [5]. However, with more women delaying childbearing for personal and professional reasons, the prevalence of PABC may rise in the future. Due to the limitations of current imaging methods of screening for PABC, it is essential to develop new diagnostic methods.

It is well known that nicotinamide adenine dinucleotide (phosphate) (NAD(P)H) and flavin adenine dinucleotide (FAD) act as electron carriers and take part in a variety of biochemical reactions, particularly the tricarboxylic acid cycle and oxidative phosphorylation [6,7]. The intrinsic fluorescence properties of NAD(P)H and FAD can be used to monitor metabolic status at the cellular level by fluorescence lifetime imaging microscopy (FLIM) without any sophisticated label [8]. It is known that the fluorescence lifetimes of NAD(P)H and FAD depend on the binding to proteins. Free NAD(P)H has a short fluorescence lifetime of about 0.3–0.6 ns, while bound NAD(P)H has increased fluorescence lifetime of 1–4 ns. The ratio of free and bound NAD(P)H is related with the types of the metabolism. For FAD, unbound FAD has a lifetime of a few ns, and bound FAD of a few 100 ps. FLIM is independent of fluorophore concentration, excitation intensity, and optical path length, which allows the visualization of fluorophore lifetime, as well as its interaction with the biological environment. FLIM has been used to study the difference between precancerous and cancerous cells [7] and to detect various malignancies in unstained human tissues [8–12]. As an important medium circulating in the whole body, blood carries a lot of information about infection, brain injuries, and cancers [13], including protein markers and circulating tumor DNA. The fluorescence spectroscopy of blood plasma has been reported as fingerprints of glucose metabolism in a rat model [14]. So far, there is limited information on the metabolic state of PABC patients' blood samples. In this study, we studied blood samples from a PABC patient and compared them with the normal cases by label-free FLIM, as well as placental tissues, to display the difference of the metabolic status between PABC and normal cases.

## 2. Materials and Methods

### 2.1. Sample Preparation

This study was approved by the Institutional Ethic Committee of the Central Hospital of Wuhan, Tongji Medical College, Huazhong University of Science and Technology. Blood and placenta tissue samples were provided by the Central Hospital of Wuhan. The samples included maternal blood, umbilical cord blood, and placental tissue sections from one PABC and seven normal parturients, whose age was between 26 and 29 years old. All the neonates had Apgar scores of 10. The PABC case in this study was not treated for breast cancer before delivery. The hematocrit and blood cell counts did not show difference for all the cases. Red blood cells (RBCs) are approximately 7.5  $\mu\text{m}$  in diameter and with average concentration of  $3.5\text{--}6.0 \times 10^6/\mu\text{L}$ . White blood cells (WBCs) are classified into five types, in which neutrophils are the predominant WBCs in adults and with a diameter of 7–18  $\mu\text{m}$  [15]. The normal concentration of WBCs is approximately  $3.6\text{--}10 \times 10^3/\mu\text{L}$ , much lower than that of RBCs. Platelets are small and irregular cells with a diameter of 2–4  $\mu\text{m}$  and normal concentration is between  $1 \times 10^5/\mu\text{L}$  and  $3 \times 10^5/\mu\text{L}$ .

Maternal blood collection was conducted from the antecubital vein after overnight fasting with vacuum blood tubes containing ethylenediaminetetraacetic acid (EDTA) dipotassium salt before delivery, and cord blood samples were collected from the umbilical cord with vacuum blood tubes after delivery. All the maternal and umbilical cord blood samples were kept at 4 °C before observation during transportation within three days for the PABC case and the FLIM laboratory are in two cities. About 3  $\mu\text{L}$  of blood was smeared on glass slides for the FLIM observation. In order to study the influence of time on the autofluorescence of blood, fresh antecubital vein blood samples from eight patients without malignant

tumors were collected at the local hospital and studied every day for 7 days. The samples were stored at 4 °C.

The placental tissue samples were freshly collected after cesarean delivery as the conventional protocol. Briefly, tissues were placed into 10% formalin for fixation, processed with ethanol and xylene (70% ethanol for 1 h, 95% ethanol for 1 h, 100% ethanol for 1 h, xylene for 100 min twice), and then placed in paraffin wax at 60 °C for 90 min 2 times. The paraffin-embedded samples were cut into slices of 4 µm thickness and placed on glass without staining for the FLIM study.

## 2.2. FLIM Setup

Blood samples were excited by a 405 nm picosecond laser (BDL-405-SMC, Becker & Hickl, Berlin, Germany) and imaged with a confocal laser scanning microscope (FV300/IX71, Olympus, Japan) and a time correlated single photon counting (TCSPC) system (SPC-150, Becker & Hickl, Germany), with a 60× water-dipping objective (NA = 1.2). The schematic design of the FLIM optical system is shown in Figure 1. Autofluorescence signal was collected by a photomultiplier tube (PMC-100-1, Becker & Hickl, Germany) with a 417–477 nm bandpass filter for NAD(P)H and a 532 nm long-pass filter for FAD. Each FLIM image has 256 × 256 pixels, and each sample was measured by FLIM for NAD(P)H at 5–6 different areas and for FAD at other 5–6 areas. Fluorescence lifetime imaging of placental tissue was acquired using Leica TCS SP8 DIVE FALCON (Leica, Berlin, Germany), equipped with a 63× water-dipping objective (NA = 1.2) and excited by a femtosecond pulsed laser of 810 nm (InSight X3 Dual, Spectra-Physics, Santa Clara, CA, USA). The emission window was set as 417–477 nm for NAD(P)H and 532–632 nm for FAD.

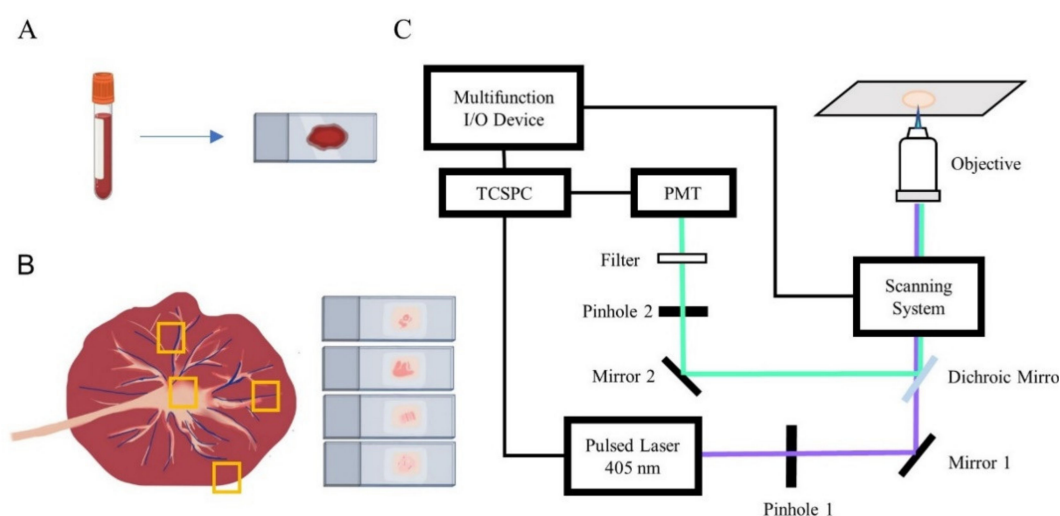


**Figure 1.** Diagram of sample preparation and equipment. (A) Preparation of blood glass smear. (B) Schematic diagram of placental sampling at various sites as marked by the yellow boxes. (C) FLIM setup.

According to the excitation spectra of NAD(P)H and FAD, the 375 nm lasers are found reasonable for excitation. However, scanners of most confocal laser scanning microscopes and microscope objectives are not designed for these wavelengths. Therefore, the 405 nm laser was used instead. For instance, Madhuri et al. observed an emission peak around 460 nm of NAD(P)H with 405 nm excitation for human blood plasma [16]. Bhatta et al. excited yeast cells with 405 nm and observed the autofluorescence of flavins compounds [17]. Becker et al. reported FLIM of FAD with 405 nm excitation and 490 to 600 nm emission filter [18].

## 2.3. Image and Data Processing

The fluorescence lifetime data obtained by the Olympus microscope was analyzed by a double-exponential decay fitting method with the software SPCImage (Becker & Hickl,

Germany). The FLIM data obtained by the Leica microscope was fitted with the software LAS X (Leica Microsystems, Berlin, Germany).

The mean fluorescence lifetime was calculated as:

$$t_m = a_1 t_1 + a_2 t_2, \quad (1)$$

where  $t_m$  is the mean lifetime,  $t_{1,2}$  are two lifetime components, and  $a_{1,2}$  are the proportion of the components. For NAD(P)H, free NAD(P)H has a short lifetime, as previously reported and measured by a free NADH solution,  $t_1$ , around 460 ps [19]; and bound NAD(P)H has a long lifetime,  $t_2$ , ranging between 1.0 and 5.7 ns, when binding to different proteins [20]. For FAD, bound FAD has a short lifetime,  $t_1$ , of a few hundred ps, while free FAD has a longer lifetime of  $t_2$  around 2730 ps [21]. When fitting with a double exponential decay,  $t_1$  of NAD(P)H and  $t_2$  of FAD were fixed, and then the  $t_m$  and  $a_{1,2}$  of all pixels were calculated. The  $t_m$  or  $a_{1,2}$  distribution curve of the  $256 \times 256$  pixels in each FLIM image can be obtained by the SPCImage software (SPCImage 8.0, Becker & Hickl, Germany). The multi-peaks of the lifetime distribution curve are fitted using a Gaussian function for each FLIM image, and at least five images are studied for each sample and averaged for statistics.

### 3. Results

#### 3.1. FLIM of NAD(P)H in Blood

For the NAD(P)H FLIM study, a representative mean lifetime ( $t_m$ ) image of normal maternal blood (Figure 2A) demonstrated the blood cells in orange, and plasma in green and blue, indicating a longer lifetime in plasma than in blood cells. The situation of PABC maternal blood was different (Figure 2B), and mainly displayed orange and yellow, representing a shorter lifetime than that in the normal group. Figure 2C shows the  $t_m$  distribution curves of Figure 2A,B. The normal curve had a relatively wider range than that of PABC. For the normal curve, two peaks can be fitted as peak 1 at 589 ps and peak 2 at 743 ps. It is noticed that peak 1 is close to the distribution of the PABC curve, with only one peak at 568 ps. The height of peak 2 in the normal group is about 8.7 times of that from PABC (Figure 2C). Figure 2D,E display the percentage of bound NAD(P)H, indicated as  $a_2$ , for normal and PABC. The blood cells shown in red had  $a_2$  less than 5%, and the plasma shown in green and blue had  $a_2$  values ranging from 5% to 30% for the normal sample. For PABC, the plasma's  $a_2$  was mostly in green (5–10%), which is significantly lower than that of normal. The distribution curves of NAD(P)H- $a_2$  (Figure 2F) showed three peaks for the normal sample, around 2%, 6%, and 14%. However, the distribution curve of PABC had two peaks (2% and 6%). The significant difference between PABC and normal was that the normal curve had a broad peak at 14%, while PABC had little distribution there (peak 3 in Figure 2F). This may partly explain why the normal NAD(P)H- $t_m$  is relatively wider than that of PABC. The NAD(P)H FLIM images and distribution curves of umbilical cord blood samples were similar to the corresponding maternal blood results (Figure 2G–L).

Figure 3 shows the statistical data of the NAD(P)H FLIM of blood, including one PABC case and seven normal cases (noted as N1–N7). The heights of peak 2 marked in Figure 2C,I and the heights of peak 3 in Figure 2F,L were analyzed and averaged from five FLIM images for each sample. It was found that the values of the normal group were significantly higher than that of PABC. Although there was individual variation among the seven normal cases, the average heights of peak 2 of the  $t_m$  curves were  $6.6 \pm 1.8$  times and  $11.9 \pm 4.3$  times that of PABC for maternal blood and cord blood, respectively. Meanwhile, the average heights of peak 3 of the  $a_2$  curves for the normal group were  $7.6 \pm 2.4$  and  $144.1 \pm 57.2$  times higher than that of PABC for maternal and cord blood, respectively.

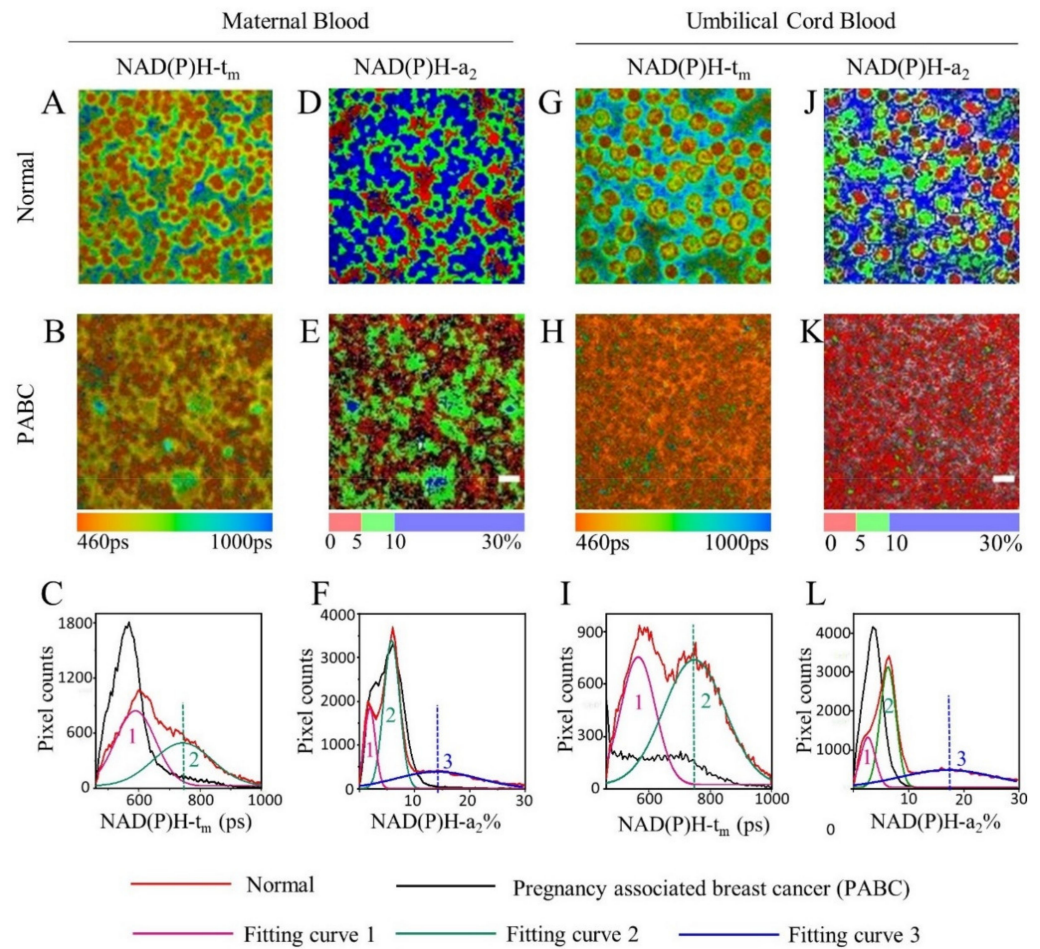


**Figure 2.** Representative NAD(P)H FLIM images and their distribution curves of normal and PABC cases. (A,B,D,E)  $t_m$  and  $a_2$  images of maternal blood, (G,H,J,K)  $t_m$  and  $a_2$  images of umbilical cord blood. (C,F,I,L) Distribution curves of corresponding images. Scale bar: 10  $\mu$ m.

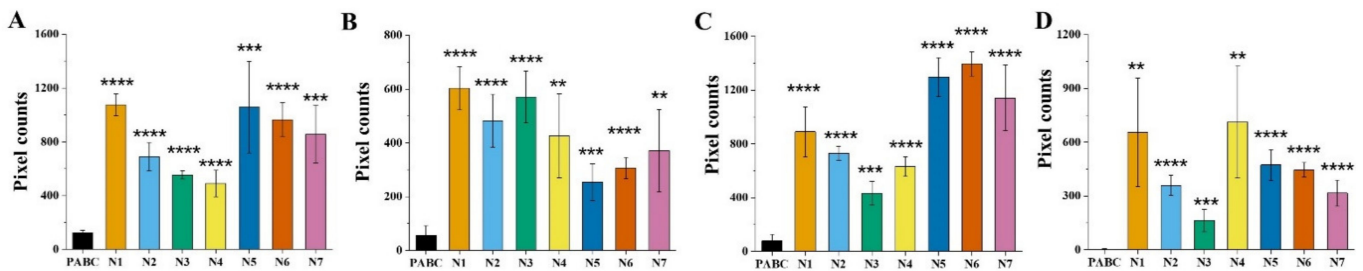


**Figure 3.** The average NAD(P)H  $t_m$  and  $a_2$  distribution curve peak heights of PABC and the normal group (including seven pairs of normal maternal blood and umbilical cord blood, N1-N7). (A) NAD(P)H- $t_m$  peak 2 height in maternal blood, (B) NAD(P)H- $a_2$  peak 3 height in maternal blood, (C) NAD(P)H- $t_m$  peak 2 height in cord blood, and (D) NAD(P)H- $a_2$  peak 3 height in cord blood (\*\*  $p < 0.01$ , \*\*\*  $p < 0.001$ , \*\*\*\*  $p < 0.0001$ ).

The PABC case had a lower NAD(P)H  $t_m$  and  $a_2$ , indicating that the metabolic pathway may have a change towards glycolysis [22]. This result is consistent with a number of studies in cultured cancer cells [23] and in cancer tissues [10,11,24]. The similar characteristics in Figure 2F,L indicate that the metabolic status of cord blood and corresponding maternal blood is similar for both normal women and the patient with PABC. It suggested that metabolic status of cord blood was correlated with that of maternal blood. As reported in a previous study [25], placental metastases may occur. In this study, the PABC placenta looked histologically normal (Figure S1) as normal cases, and no detectable metabolic

difference in the placenta was found between the PABC case and normal cases. Although no metastasis was observed in the placenta for this PABC case, the cord blood from the PABC case may be affected by abnormal maternal metabolism through the placenta.

### 3.2. FLIM of FAD in Blood

FAD is also an important coenzyme in metabolism. Representative FAD mean lifetime ( $t_m$ ) and percentage of bound-FAD ( $a_1$ ) images of PABC and normal blood samples were compared (Figure 4). The FAD- $t_m$  of maternal blood in PABC is shorter than that of normal, especially in plasma (Figure 4A,B). Figure 4C displays the  $t_m$  distribution curves of Figure 4A,B. PABC had a single narrow peak at 557 ps, which overlapped with peak 1 of the normal curve, but was nearly absent at peak 2 of normal curve (Figure 4C).

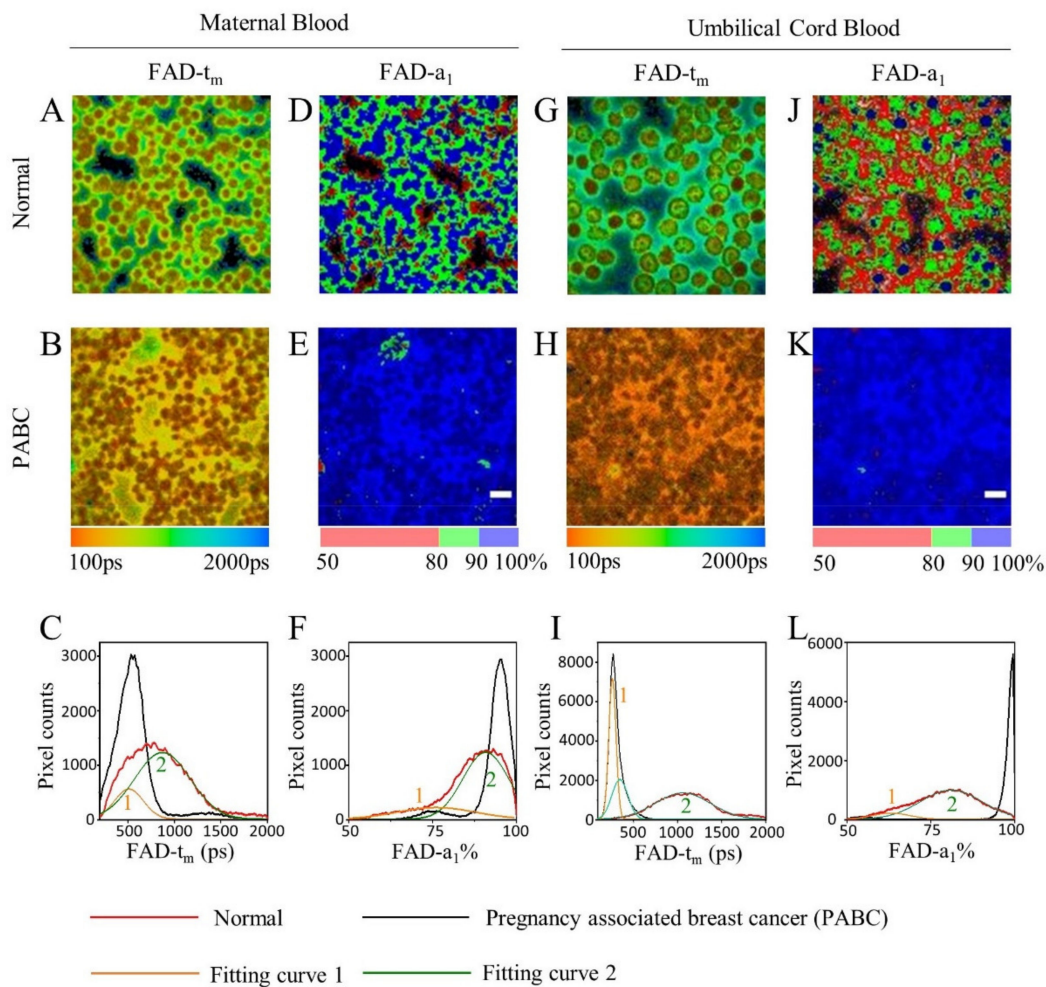


**Figure 4.** Representative FAD FLIM images and their distribution curves of PABC and normal cases. (A,B,D,E)  $t_m$  and  $a_1$  images of maternal blood, (G,H,J,K)  $t_m$  and  $a_1$  images of umbilical cord blood. (C,F,I,L) Distribution curves of corresponding images. Scale bar: 10  $\mu\text{m}$ .

Peak 2 in normal cases may originate from the fluorescence in plasma. Figure 4D shows that FAD- $a_1$  of normal maternal blood cells was higher than 90%, while that of plasma decreased to 50–90%. In contrast, for PABC, FAD- $a_1$  values of both blood cells and plasma were more than 90% (Figure 4E). The  $a_1$  distribution curve demonstrated that the full width at half maximum (FWHM) of the normal maternal blood group is 2.8 times that in the PABC case (Figure 4F). This indicates that there is a difference in FAD status between blood cells and plasma in normal maternal blood, while the FAD status in the PABC blood sample has undergone major changes. With the bound-FAD ratio increased in PABC, the FAD- $t_m$  was slightly smaller, and the distribution was narrower. The FAD images and

distribution characteristics of umbilical cord blood were similar to those of maternal blood, as shown in Figure 4G–L.

Statistical analyses of the FWHM of the peaks in Figure 4C–L were performed, as well as of the other FLIM images. At least five FLIM images of each sample were analyzed, and the averaged FWHM values are displayed in Figure 5. The maternal blood distributions of FAD- $t_m$  and FAD- $a_1$  in the normal group were significantly wider than those in the PABC case ( $p < 0.01$ ), and their FWHMs were  $2.3 \pm 0.6$  times and  $2.8 \pm 0.6$  times that from PABC, respectively. The gap in cord blood samples was even greater. The FWHM of normal cord blood  $t_m$  and  $a_1$  were  $5.0 \pm 1.1$  times and  $9.7 \pm 2.8$  times that of PABC, respectively.

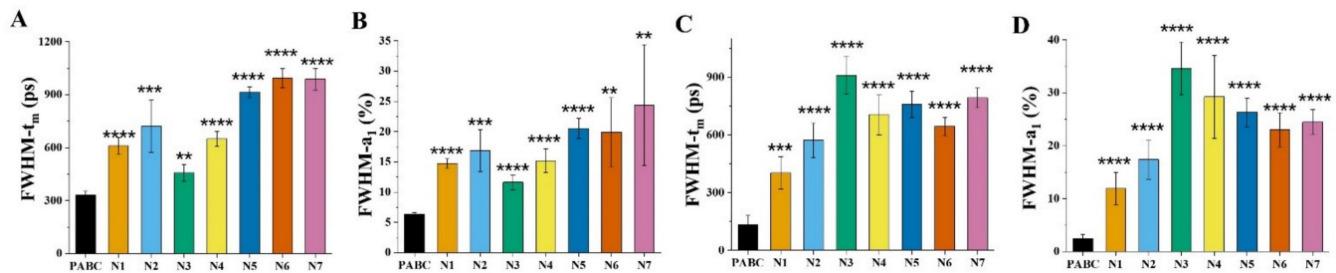


**Figure 5.** The FWHM of the FAD  $t_m$  and  $a_1$  distribution curves of PABC and the normal group (including seven pairs of normal maternal blood and umbilical cord blood, N1–N7). (A) FAD- $t_m$  of maternal blood, (B) FAD- $a_1$  of maternal blood, (C) FAD- $t_m$  of cord blood, (D) FAD- $a_1$  of cord blood (\*\*  $p < 0.01$ , \*\*\*  $p < 0.001$ , \*\*\*\*  $p < 0.0001$ ).

The FAD data of blood showed that both maternal and cord blood of PABC had shorter mean lifetimes and higher bound-FAD ratios. The metabolic states in plasma and blood cells of PABC were similar, so the distribution was more concentrated than normal cases.

The influence of time on the autofluorescence of blood samples from eight patients without malignant tumors were studied over seven days. Figure S2 presented an example of one antecubital vein blood sample, and Figure S2A,B showed a group of  $t_m$  and  $a_2$  distribution curves of NAD(P)H FLIM images within seven days. There are small changes among the curves from fresh samples to stored for seven days. All the other seven blood samples are similar with typical curves in Figure S2. Since the statistical analysis (Figure 3) was based on the height of NAD(P)H- $t_m$  peak 2 and NAD(P)H- $a_2$  peak 3 in Figure 2, the height of corresponding peaks in Figure S2A,B were analysed as well and the averaged values were displayed in Figure S2C,D. For comparison, the peak height of the PABC case was also shown. It can be seen that all the peak heights of the control group (tumor-free patients) stored for 0–6 days were much higher than the results of PABC. Similar results can be found for FAD in Figure S3. Therefore, the influence of time on the NAD(P)H and FAD fluorescence of blood is negligible in this work.

#### 4. Discussion

PABC is a rare disease. As reported in a population-based cohort study on 8.8 million births, an overall 10-year incidence of PABC is 6.5 cases per 100,000 births [2]. This rare case has only been found once in the hospital where the authors work for decades. Therefore, the cohort in this study is small. Fortunately, for this PABC patient, there are two blood samples—maternal blood and umbilical cord blood. The umbilical cord blood samples showed similar metabolic status results, compared to the corresponding maternal blood results, whether it is from the PABC patient or from the normal group. It suggested that metabolic status of cord blood was correlated with that of maternal blood. Nevertheless, more PABC cases' study would be useful to clarify the differences between PABC and normal cases.

Despite extensive researches on FLIM in the medical field to characterize cellular and tissular metabolic changes for cancer, only a handful of published studies have reported on the NAD(P)H and FAD in blood for cancer detection. Kalaivani et al. found a difference in blood obtained from cervical cancer patients and normal controls by time-resolved

spectra [24]. Organs can interact with the blood circulation. It was reported that NAD (NAD<sup>+</sup> and NADH) concentrations decreased both in blood and tissues (including liver, kidney, stomach, cerebrum, lung, spleen, and large and small intestine) when mice were fed a NiA-free diet [26]. It was also reported that NADH together with SIRT protein promote tumorigenesis [27]. It could be assumed that PABC disease influences NAD(P)H in blood as well.

Blood is composed of a variety of components, including RBCs, WBCs, platelets, and plasma. According to the size of blood cells and their average concentrations, most of the blood cells shown in Figures 2 and 4 are RBCs. As presented in Figure S4, a few cells were observed with larger size and different fluorescence lifetimes than RBCs, which might be WBCs. The metabolism of RBCs indirectly mirrors systemic metabolic status as they circulate in the bloodstream, owing to the abundance of metabolite transporters in RBC membranes [28]. The metabolites in RBCs involved in glycolysis and Krebs cycle were studied, and some of them were found to be a signal and mediator in the whole organism, including muscles, liver, brain, and cancer cells [29]. The NAD concentration was reported in the range of 10–60  $\mu$ M in human RBCs [30], while the concentration in blood plasma varies in different reports [31,32]. Therefore, both intracellular and extracellular NAD(P)H of blood samples should be studied for metabolism. In the present study, whole blood with a small amount was tested for each sample. No centrifugation operation was needed and the autofluorescence from both blood cells and blood plasma was detected. The NAD(P)H mean lifetime ( $t_m$ ) of PABC blood was shorter than that of normal blood (Figure 2C). The bound-NAD(P)H proportion ( $a_2$ ) of PABC blood was significantly lower than that of normal (Figure 2F). Similar results have been reported in many cancer tissues, such as breast cancer [8,20,33], cervical cancer [10,24], and lung cancer [11]. Most reports have suggested that this phenomenon was caused by the Warburg effect [34]; that is, cell carcinogenesis promoted a metabolic shift to glycolysis, with oxidative phosphorylation inhibited, thus reducing the fluorescence lifetime of NAD(P)H and the proportion of bound NAD(P)H. In order to meet the need for rapid synthesis of nucleic acids and fatty acids and maintain a reduced state in fast-dividing cancer cells, some changes may occur in the metabolic pathways of cancer cells, including increasing the pentose phosphate pathway (PPP) [35]. The PPP specifically produces NADPH, which leads to an increase in the free NADPH pool and a decrease in the proportion of bound NADPH. In addition, immune cells and tumor cells are in a tumor microenvironment and have similar physical stresses, glycolysis metabolism, and the Warburg effect are also found valid for myeloid cells and lymphoid cells, i.e., macrophages, and mainly for circulating lymphocytes, even more than for RBCs [36]. It was reported that tumor acidity and altered nutrient availability affected the metabolic reprogramming of T lymphocytes, resulting in differentiation towards suppressive phenotypes [37]. The metabolic profiles of cancer cells and activated T lymphocytes are remarkably similar [37]. Macrophage activity against pathogens and tumor cells requires aerobic glycolysis, which is required for both the M1 and M2 polarization state of macrophages [38]. Glucose levels in the tumor microenvironment due to high glucose consumption alter the activation status of tumor-associated macrophages and drive the metabolic changes and a switch to glycolytic metabolism in macrophages [39]. Thus, the role of a variety of blood cells should be considered to study the metabolic changes.

FAD is another redox cofactor mainly localized in mitochondria, also some in the nuclei and cytosolic compartment; besides, the HPLC experiments showed that rat liver nuclei contain protein-bound FAD [40]. Even though RBCs do not have nuclear or mitochondria, they still contain FAD. The FAD mean lifetime ( $t_m$ ) of maternal and cord blood from PABC is shorter than that from the normal group, and the proportion of bound-FAD ( $a_2$ ) in PABC blood is higher than that of the normal group (Figure 4). This result is consistent with our previous report of human lung cancer tissues and cultured human bronchial epithelial cells (BEAS-2B) [11]. That is, the fluorescence lifetime of human lung cancer tissue was shorter than that of normal lung tissue, and the fluorescence lifetimes of both NAD(P)H and FAD in BEAS-2B cells decreased when inhibiting cell oxidative phosphorylation. As

previously reported [29], RBCs can be impacted by systemic metabolic homeostasis and other cell functions, and are found involved in inflammation, neurodegenerative diseases, aging, and cancer. As discussed above, other blood cells as macrophages and lymphocytes can also reflect the metabolic changes of tumor microenvironment and are impacted by metabolic changes, even more than RBCs. We hypothesize that the metabolic change of PABC would indirectly response in the variety of blood cells and plasma. The FAD results (Figures 4 and 5) indicated that the glycolysis pathway may be more dominant in the PABC case due to the Warburg effect, resulting in the decrease of the fluorescence lifetime of NAD(P)H and FAD, either in cancer cells or in blood. It has been reported that the riboflavin levels, the coenzyme activation of erythrocyte glutathione reductase [41], fructose and glucose concentrations [42], glucose and glycosylated haemoglobin levels [43] in maternal blood and cord blood showed significant correlation. In this work, the FAD difference both in maternal blood and cord blood might be caused by the correlation between them as well. However, the FAD result is different from a few reports on cancer tissues or cancer cells. For example, an increase in FAD lifetime was observed in highly cancerous epithelial cells in a hamster oral model [44] and in human pancreatic cancer tissues [45] than in normal cells or tissues. Since the microenvironment of a tumor is quite complicated, the changes of the microcirculation and the partial oxygen pressure will vary greatly with the location of the cancer cells and the cancer development progress. The metabolic pathway of tumor cells can shift between glycolysis and oxidative phosphorylation [46,47]. Therefore, it is possible to find different trends of the FAD fluorescence lifetime in different cancer diseases.

Although maternal cancer during pregnancy is rare, metastatic maternal malignancy to the placenta and/or fetus have been reported more than 100 cases in recent decades [48]. Froehlich et al. reported a case of PABC with the large amount of placenta metastases, and cancer cells were observed only in the placental intervillous space, but not in the villi or other extraembryonic fetal tissues [25]. Miller et al. reported a case of rapidly progressive and fatal gastric carcinoma during pregnancy, with spread to the maternal blood space within the placenta but no chorionic villous invasion [48]. It is likely that placental metastases are more common than reported, especially with a lack of or inadequate pathologic examination of placentas [49]. In this study, the PABC placenta looked histologically normal (Figure S1), and no detectable difference in the placenta was found between the PABC and normal cases by two-photon excitation FLIM. The major advantage of two-photon excitation is the greater depth of tissue penetration compared with the single-photon excitation. For tissue study, especially those thick tissue that cannot be sliced, two-photon excitation is more appropriate. Considering the potential placental and fetal metastasis, it is of importance to examine the placenta carefully for pregnancy-related cancer even if macroscopic inspection is normal.

## 5. Conclusions

In summary, this study performed a FLIM study to detect metabolic status by NAD(P)H and FAD fluorescence in maternal blood and cord blood from a PABC case, and compared with seven normal cases. It was found that the metabolic status of maternal blood and the corresponding cord blood were similar for either the PABC case or the normal group. More importantly, the mean lifetimes of NAD(P)H and FAD in PABC blood were lower than in the normal group, and the FAD distribution range of PABC was much narrower than that of the normal group. The results of the reported PABC case suggest the use of FLIM testing to identify metabolic changes in PABC and support further analysis in a larger sample size.

**Supplementary Materials:** The following are available online at <https://www.mdpi.com/article/10.3390/diagnostics11081494/s1>, Figure S1: FLIM images of an unstained placenta slice of the PABC case and no metastasis was observed in the placenta, Figure S2: The storage time influence on the NAD(P)H lifetime of blood samples, Figure S3: The storage time influence on the FAD lifetime of blood samples, Figure S4: NAD(P)H FLIM images of maternal blood samples showing that some cells (marked with arrows) might be WBCs.

**Author Contributions:** Conceptualization, L.M. and Y.W.; methodology, L.Z. and L.M.; software, Y.K. and J.W.; validation and formal analysis, L.Z., J.W. and X.L.; resources, Y.F., J.M., and Y.W.; data curation, J.W. and X.L.; writing—original draft preparation, L.Z.; writing—review and editing, Y.W. and L.M.; supervision, L.M.; project administration, L.M.; funding acquisition, Y.F., J.M., and L.M. All authors have read and agreed to the published version of the manuscript.

**Funding:** This work was financially supported by Medical Engineering Fund of Fudan University (yg2021-022), Fudan University-CIOMP Joint Fund (FC2018-001), Pioneering Project of Academy for Engineering and Technology of Fudan University (gyy2018-001, gyy2018-002), Shanghai Natural Science Foundation (grant No. 20ZR1405100, 20ZR1403700), Science and Technology Research Program of Shanghai (grant No. 19DZ2282100), Shanghai key discipline construction plan (2020-2022) (grant No. GWV-10.1-XK01), and Shanghai Engineering Technology Research Center of Hair Medicine (19DZ2250500).

**Institutional Review Board Statement:** The study was conducted according to the guidelines of the Declaration of Helsinki, and approved by the Institutional Ethic Committee of the Central Hospital of Wuhan, Tongji Medical College, Huazhong University of Science and Technology ((2020) IEC(A212) on 6 April 2020).

**Informed Consent Statement:** Written informed consent was obtained from the patients to publish this paper.

**Data Availability Statement:** Data are available from the corresponding author upon reasonable request.

**Acknowledgments:** We thank all the faculty and staff at the Department of Gynecology and Obstetrics, The Central Hospital of Wuhan, Tongji Medical College, Huazhong University of Science and Technology for their clinical support.

**Conflicts of Interest:** The authors declare no conflict of interest. The funders had no role in the design of the study; in the collection, analyses, or interpretation of data; in the writing of the manuscript, or in the decision to publish the results.

## References

1. Sung, H.; Ferlay, J.; Siegel, R.L.; Laversanne, M.; Soerjomataram, I.; Jemal, A.; Bray, F. Global cancer statistics 2020: GLOBOCAN estimates of incidence and mortality worldwide for 36 cancers in 185 countries. *CA-Cancer J. Clin.* **2021**, *71*, 209–249. [[CrossRef](#)]
2. Abenhaim, H.A.; Azoulay, L.; Holcroft, C.A.; Bure, L.A.; Assayag, J.; Benjamin, A. Incidence, risk factors, and obstetrical outcomes of women with breast cancer in pregnancy. *Breast J.* **2012**, *18*, 564–568. [[CrossRef](#)]
3. Ahn, B.Y.; Kim, H.H.; Moon, W.K.; Pisano, E.D.; Kim, H.S.; Cha, E.S.; Kim, J.S.; Oh, K.K.; Park, S.H. Pregnancy- and lactation-associated breast cancer: Mammographic and sonographic findings. *J. Ultrasound Med.* **2003**, *22*, 491–497. [[CrossRef](#)]
4. Amant, F.; Loibl, S.; Neven, P.; Van Calsteren, K. Breast cancer in pregnancy. *Lancet* **2012**, *379*, 570–579. [[CrossRef](#)]
5. Collins, L.C.; Gelber, S.; Marotti, J.D.; White, S.; Ruddy, K.; Brachtel, E.F.; Schapira, L.; Come, S.E.; Borges, V.F.; Schedin, P.; et al. Molecular Phenotype of Breast Cancer According to Time Since Last Pregnancy in a Large Cohort of Young Women. *Oncologist* **2015**, *20*, 713–718. [[CrossRef](#)] [[PubMed](#)]
6. Katsyuba, E.; Romani, M.; Hofer, D.; Auwerx, J. NAD<sup>+</sup> homeostasis in health and disease. *Nat. Metab.* **2020**, *2*, 9–31. [[CrossRef](#)] [[PubMed](#)]
7. Skala, M.C.; Ricking, K.M.; Gendron-Fitzpatrick, A.; Eickhoff, J.; Eliceiri, K.W.; White, J.G.; Ramanujam, N. In vivo multiphoton microscopy of NADH and FAD redox states, fluorescence lifetimes, and cellular morphology in precancerous epithelia. *Proc. Natl. Acad. Sci. USA* **2007**, *104*, 19494–19499. [[CrossRef](#)] [[PubMed](#)]
8. Conklin, M.W.; Provenzano, P.P.; Eliceiri, K.W.; Sullivan, R.; Keely, P.J. Fluorescence lifetime imaging of endogenous fluorophores in histopathology sections reveals differences between normal and tumor epithelium in carcinoma in situ of the breast. *Cell Biochem. Biophys.* **2009**, *53*, 145–157. [[CrossRef](#)] [[PubMed](#)]
9. Huang, M.; Zhang, Z.; Wang, X.; Xie, Y.; Fei, Y.; Ma, J.; Wang, J.; Chen, L.; Mi, L.; Wang, Y. Detecting benign uterine tumors by autofluorescence lifetime imaging microscopy through adjacent healthy cervical tissues. *J. Innov. Opt. Health Sci.* **2019**, *12*, 1940006. [[CrossRef](#)]
10. Wang, X.; Wang, Y.; Zhang, Z.; Huang, M.; Fei, F.; Ma, J.; Mi, L. Discriminating different grades of cervical intraepithelial neoplasia based on label-free phasor fluorescence lifetime imaging microscopy. *Biomed. Opt. Express* **2020**, *11*, 1977–1990. [[CrossRef](#)] [[PubMed](#)]
11. Wang, M.; Tang, F.; Pan, X.; Yao, L.; Wang, X.; Jing, Y.; Ma, J.; Wang, G.; Mi, L. Rapid diagnosis and intraoperative margin assessment of human lung cancer with fluorescence lifetime imaging microscopy. *BBA Clin.* **2017**, *8*, 7–13. [[CrossRef](#)]
12. Liu, L.; Yang, Q.; Zhang, M.; Wu, Z.; Xue, P. Fluorescence lifetime imaging microscopy and its applications in skin cancer diagnosis. *J. Innov. Opt. Health Sci.* **2019**, *12*, 1930004. [[CrossRef](#)]

13. Sohn, E. Diagnosis: Frontiers in blood testing. *Nature* **2017**, *549*, S16–S18. [[CrossRef](#)] [[PubMed](#)]
14. Shirshin, E.; Cherkasova, O.; Tikhonova, T.; Berlovskaya, E.; Priezzhev, A.; Fadeev, V. Native fluorescence spectroscopy of blood plasma of rats with experimental diabetes: Identifying fingerprints of glucose-related metabolic pathways. *J. Biomed. Opt.* **2015**, *20*, 051033. [[CrossRef](#)] [[PubMed](#)]
15. Kuan, D.-H.; Wu, C.-C.; Su, W.-Y.; Huang, N.-T. A Microfluidic Device for Simultaneous Extraction of Plasma, Red Blood Cells, and On-Chip White Blood Cell Trapping. *Sci. Rep.* **2018**, *8*, 15345. [[CrossRef](#)]
16. Madhuri, S.; Vengadesan, N.; Aruna, P.; Koteswaran, D.; Venkatesan, P.; Ganesan, S. Native fluorescence spectroscopy of blood plasma in the characterization of oral malignancy. *Photochem. Photobiol.* **2003**, *78*, 197–204. [[CrossRef](#)]
17. Bhatta, H.; Goldys, M.E. Characterization of yeast strains by fluorescence lifetime imaging microscopy. *FEMS Yeast Res.* **2008**, *8*, 81–87. [[CrossRef](#)]
18. Becker, W.; Bergmann, A.; Ibarrola, S.R.; Müller, P.-F.; Braun, L. Metabolic imaging by simultaneous FLIM of NAD(P)H and FAD. In *Multiphoton Microscopy in the Biomedical Sciences XIX, Proceedings of the SPIE BiOS SPIE, San Francisco, CA, USA, 2–7 February 2019*; SPIE: Bellingham, WA, USA, 2019; p. 108820B.
19. Guo, K.; Wu, J.; Kong, Y.; Zhou, L.; Li, W.; Fei, Y.; Ma, J.; Mi, L. Label-free and noninvasive method for assessing the metabolic status in type 2 diabetic rats with myocardium diastolic dysfunction. *Biomed. Opt. Express* **2021**, *12*, 480–493. [[CrossRef](#)] [[PubMed](#)]
20. Tadrous, P.J.; Siegel, J.; French, P.M.W.; Shousha, S.; Lalani, E.-N.; Stamp, G.W.H. Fluorescence lifetime imaging of unstained tissues: Early results in human breast cancer. *J. Pathol.* **2003**, *199*, 309–317. [[CrossRef](#)]
21. Kolenc, O.I.; Quinn, K.P. Evaluating Cell Metabolism Through Autofluorescence Imaging of NAD(P)H and FAD. *Antioxid. Redox. Signal* **2019**, *30*, 875–889. [[CrossRef](#)]
22. Bird, D.K.; Yan, L.; Vrotsos, K.M.; Eliceiri, K.W.; Vaughan, E.M.; Keely, P.J.; White, J.G.; Ramanujam, N. Metabolic mapping of MCF10A human breast cells via multiphoton fluorescence lifetime imaging of the coenzyme NADH. *Cancer Res.* **2005**, *65*, 8766–8773. [[CrossRef](#)]
23. Alhallak, K.; Rebello, L.G.; Muldoon, T.J.; Quinn, K.P.; Rajaram, N. Optical redox ratio identifies metastatic potential-dependent changes in breast cancer cell metabolism. *Biomed. Opt. Express* **2016**, *7*, 4364–4374. [[CrossRef](#)]
24. Kalaivani, R.; Masilamani, V.; AlSalhi, M.S.; Devanesan, S.; Ramamurthy, P.; Palled, S.R.; Ganesh, K.M. Cervical cancer detection by time-resolved spectra of blood components. *J. Biomed. Opt.* **2014**, *19*, 057011. [[CrossRef](#)]
25. Froehlich, K.; Stensheim, H.; Markert, U.R.; Turowski, G. Breast carcinoma in pregnancy with spheroid-like placental metastases—a case report. *APMIS* **2018**, *126*, 448–452. [[CrossRef](#)] [[PubMed](#)]
26. Terakata, M.; Fukuwatari, T.; Sano, M.; Nakao, N.; Sasaki, R.; Fukuoka, S.-I.; Shibata, K. Establishment of true niacin deficiency in quinolinic acid phosphoribosyltransferase knockout mice. *J. Nutr.* **2012**, *142*, 2148–2153. [[CrossRef](#)] [[PubMed](#)]
27. Becherini, P.; Caffa, I.; Piacente, F.; Damonte, P.; Vellone, V.G.; Passalacqua, M.; Benzi, A.; Bonfiglio, T.; Reverberi, D.; Khalifa, A.; et al. SIRT6 enhances oxidative phosphorylation in breast cancer and promotes mammary tumorigenesis in mice. *Cancer Metab.* **2021**, *9*, 6. [[CrossRef](#)] [[PubMed](#)]
28. Culp-Hill, R.; Zheng, C.; Reisz, A.J.; Smith, K.; Rachubinski, A.; Nemkov, T.; Butcher, E.; Granrath, R.; Hansen, C.K.; Espinosa, M.J.; et al. Red blood cell metabolism in Down syndrome: Hints on metabolic derangements in aging. *Blood Adv.* **2017**, *1*, 2776–2780. [[CrossRef](#)] [[PubMed](#)]
29. Nemkov, T.; Reisz, A.J.; Xia, Y.; Zimring, C.J.; D’Alessandro, A. Red blood cells as an organ? How deep omics characterization of the most abundant cell in the human body highlights other systemic metabolic functions beyond oxygen transport. *Expert Rev. Proteomic* **2018**, *15*, 855–864. [[CrossRef](#)]
30. Micheli, V.; Sestini, S. Determining NAD synthesis in erythrocytes. *Method Enzym.* **1997**, *280*, 211–221.
31. Brunnbauer, P.; Leder, A.; Kamali, C.; Kamali, K.; Keshi, E.; Splith, K.; Wabitsch, S.; Haber, P.; Atanasov, G.; Feldbrügge, L.; et al. The nanomolar sensing of nicotinamide adenine dinucleotide in human plasma using a cycling assay in albumin modified simulated body fluids. *Sci. Rep.* **2018**, *8*, 16110. [[CrossRef](#)]
32. O’Reilly, T.; Niven, D.F. Levels of nicotinamide adenine dinucleotide in extracellular body fluids of pigs may be growth-limiting for actinobacillus pleuropneumoniae and haemophilus parasuis. *Can. J. Vet. Res.* **2003**, *67*, 229–231.
33. Phipps, J.E.; Gorpas, D.; Unger, J.; Darrow, M.; Bold, R.J.; Marcu, L. Automated detection of breast cancer in resected specimens with fluorescence lifetime imaging. *Phys. Med. Biol.* **2017**, *63*, 015003. [[CrossRef](#)]
34. Lu, J.; Tan, M.; Cai, Q. The Warburg effect in tumor progression: Mitochondrial oxidative metabolism as an anti-metastasis mechanism. *Cancer Lett.* **2015**, *356*, 156–164. [[CrossRef](#)] [[PubMed](#)]
35. Patra, K.C.; Hay, N. The pentose phosphate pathway and cancer. *Trends Biochem. Sci.* **2014**, *39*, 347–354. [[CrossRef](#)] [[PubMed](#)]
36. Sun, L.; Suo, C.; Li, S.; Zhang, H.; Gao, P. Metabolic reprogramming for cancer cells and their microenvironment: Beyond the Warburg Effect. *BBA-Rev. Cancer* **2018**, *1870*, 51–66. [[CrossRef](#)]
37. Allison, K.; Coomber, B.; Bridle, B. Metabolic reprogramming in the tumour microenvironment: A hallmark shared by cancer cells and T lymphocytes. *Immunology* **2017**, *152*, 175–184. [[CrossRef](#)] [[PubMed](#)]
38. Mehla, K.; Singh, P. Metabolic Regulation of Macrophage Polarization in Cancer. *Trends Cancer* **2019**, *5*(12), 822–834. [[CrossRef](#)]
39. Kim, J.; Bae, J. Metabolic regulation of macrophages in tumor microenvironment. *Curr. Opin. Hematol.* **2018**, *1*, 52–59. [[CrossRef](#)]
40. Giancaspero, T.A.; Busco, G.; Panebianco, C.; Carmone, C.; Miccolis, A.; Liuzzi, G.M.; Colella, M.; Barile, M. FAD synthesis and degradation in the nucleus create a local flavin cofactor pool. *J. Biol. Chem.* **2013**, *288*, 29069–29080. [[CrossRef](#)]
41. Shaw, N.-S. Riboflavin status in late pregnancy, postpartum and cord blood. *Nutr. Res.* **1993**, *13*, 147–155. [[CrossRef](#)]

42. Trindade, E.P.C.; Barreiros, C.R.; Kurokawa, C.; Bossolan, G. Fructose in fetal cord blood and its relationship with maternal and 48-hour-newborn blood concentrations. *Early Hum. Dev.* **2011**, *87*, 193–197. [[CrossRef](#)] [[PubMed](#)]
43. Elshibly, E.M.; Atabani, G.S.; Osman, N.M.; Hassan, D.A.; Saeed, B.O.; Omer, M.I. Cord and maternal glycosylated haemoglobin levels: A study in Sudanese pregnant diabetic women. *Ann. Trop. Paediatr.* **1990**, *10*, 373–376. [[CrossRef](#)]
44. Malik, B.H.; Lee, J.; Cheng, S.; Cuenca, R.; Jabbour, J.M.; Cheng, Y.-S.L.; Wright, J.M.; Ahmed, B.; Maitland, K.C.; Jo, J.A. Objective Detection of Oral Carcinoma with Multispectral Fluorescence Lifetime Imaging In Vivo. *Photochem. Photobiol.* **2016**, *92*, 694–701. [[CrossRef](#)]
45. Shen, B.; Yan, J.; Wang, S.; Zhou, F.; Zhao, Y.; Hu, R.; Qu, J.; Liu, L. Label-free whole-colony imaging and metabolic analysis of metastatic pancreatic cancer by an autoregulating flexible optical system. *Theranostics* **2020**, *10*, 1849–1860. [[CrossRef](#)]
46. Cantor, J.R.; Sabatini, D.M. Cancer cell metabolism: One hallmark, many faces. *Cancer Discov.* **2012**, *2*, 881–898. [[CrossRef](#)]
47. Zu, X.L.; Guppy, M. Cancer metabolism: Facts, fantasy, and fiction. *Biochem. Biophys. Res. Commun.* **2004**, *313*, 459–465. [[CrossRef](#)] [[PubMed](#)]
48. Miller, K.; Zawislak, A.; Gannon, C.; Millar, D.; Loughrey, M.B. Maternal Gastric Adenocarcinoma with Placental Metastases: What Is the Fetal Risk? *Pediatr. Dev. Pathol.* **2012**, *15*, 237–239. [[CrossRef](#)] [[PubMed](#)]
49. Al-Adnani, M.; Kiho, L.; Scheimberg, I. Maternal pancreatic carcinoma metastatic to the placenta: A case report and literature review. *Pediatr. Dev. Pathol.* **2007**, *10*, 61–65. [[CrossRef](#)] [[PubMed](#)]